Current Research in Structural Biology 7 (2024) 100137

Contents lists available at ScienceDirect

Current Research in Structural Biology

journal homepage: www.journals.elsevier.com/current-research-in-structural-biology

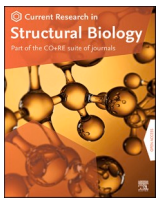

Research Article

Cholesterol modulates the structural dynamics of the paddle motif loop of KvAP voltage sensor

Anindita Das [a,b,1], Arpan Bysack [a,b,1], H. Raghuraman [a,b,*]

[a] Crystallography and Molecular Biology Division, Saha Institute of Nuclear Physics, 1/AF Bidhannagar, Kolkata, India
[b] Homi Bhabha National Institute, Training School Complex, Anushaktinagar, Mumbai, 400 094, India

ARTICLE INFO

Handling Editor: Dr CS Verma

Keywords:
Voltage sensor
KvAP
Lipid-dependent gating
Cholesterol
Membrane penetration depth

ABSTRACT

KvAP is a prokaryotic Kv channel, which has been widely used as a model system to understand voltage- and lipid-dependent gating mechanisms. In phospholipid membranes, the KvAP-VSD adopts the activated/'Up' conformation, whereas the presence of non-phospholipids in membranes favours the structural transition to resting/'Down' state. The S3b-S4 paddle motif loop of KvAP-VSD is functionally important as this participates in protein-protein interactions and is the target for animal toxins. In this study, we have monitored the modulatory role of cholesterol – the physiologically-relevant non-phospholipid – on the organization and dynamics of the S3b-S4 loop of the isolated KvAP-VSD in membranes by site-directed fluorescence approaches using the environmental sensitivity of 7-nitrobenz-2-oxa-1,3-diazol-4-yl-ethylenediamine (NBD) fluorescence. Our results show that cholesterol alters the dynamic nature (rotational and hydration dynamics) of S3b-S4 loop in a segmental fashion, *i.e.*, the residues 110 to 114 and 115 to 117 behave differently in the presence of cholesterol, which is accompanied by considerable change in conformational heterogeneity. Further, quantitative depth measurements using the parallax quenching method reveal that the sensor loop is located at the shallow interfacial region of cholesterol-containing membranes, suggesting that the sensor loop organization is not directly correlated with S4 helix movement. Our results clearly show that cholesterol-induced changes in bilayer properties may not be the predominant factor for the sensor loop's altered structural dynamics, but can be attributed to the conformational change of the KvAP-VSD in cholesterol-containing membranes. Overall, these results are relevant for gating mechanisms, particularly the lipid-dependent gating, of Kv channels in membranes.

1. Introduction

Voltage-gated K^+ (K_v) channels are transmembrane proteins that assemble as functional tetramers to regulate various physiological processes (Kim and Nimigean, 2016; Catacuzzeno and Franciolini, 2022) and are important drug targets (Wulff et al., 2009). These highly-selective ion channels contain regulatory voltage sensing domains (VSD), which sense the differences in transmembrane potential and directs the pore domain (PD) to conduct K^+ ions down the concentration gradient through electromechanical coupling (Bezanilla, 2008). The VSD is an antiparallel four-helix bundle (helices S1 to S4), containing a cluster of highly-conserved positive charges (arginine residues) in the S4 helix (Jiang et al., 2003; Bezanilla, 2008; Swartz, 2008; Catterall, 2010). Depolarization of the membrane potential induces a reorientation of a small portion of S3 and the S4 helix (S3b-S4 voltage-sensing paddle motif) within the transmembrane electric field (Long et al., 2007). This structural rearrangement has long been associated with the transition from resting ('Down') conformation to the activated ('Up') conformation of the VSD and leads to pore opening through its mechanical coupling with the S4–S5 linker between domains (Jiang et al., 2003; Bezanilla, 2008; Tombola et al., 2006; Swartz, 2008). Interestingly, not only the VSDs form an integral part of voltage-gated

Abbreviations: 5-PC, 1-palmitoyl-2-(5-doxyl)stearoyl-*sn*-glycero-3-phosphocholine; Chol, cholesterol; DOPC, 1,2-dioleoyl-*sn*-glycero-3-phosphocholine; DM, n-decyl-β-D-maltopyranoside; IPTG, isopropylthiogalactoside; MEM, maximum entropy method; NBD, 7-nitrobenz-2-oxa-1,3-diazol-4-yl-ethylenediamine; POPC, 1-palmitoyl-2-oleoyl-*sn*-glycero-3-phosphocholine; POPG, 1-palmitoyl-2-oleoyl-*sn*-glycero-3-phospho-(1′-rac-glycerol); REES, red edge excitation shift; Tempo-PC, 1,2-dioleoyl-*sn*-glycero-3-phosphotempocholine; TCSPC, time-correlated single photon counting.

* Corresponding author. Crystallography and Molecular Biology Division, Saha Institute of Nuclear Physics, 1/AF Bidhannagar, Kolkata, India.
E-mail address: h.raghuraman@saha.ac.in (H. Raghuraman).

[1] equal contribution.

https://doi.org/10.1016/j.crstbi.2024.100137
Received 29 November 2023; Received in revised form 29 February 2024; Accepted 3 March 2024
Available online 6 March 2024

ion channels, but are also found associated with voltage-dependent enzymes (Murata et al., 2005). All voltage sensors share the four-helix bundle architecture as a common scaffold as demonstrated by the structures of several voltage-gated ion channels (Jiang et al., 2003; Long et al., 2007; Payandeh et al., 2011; Zhang et al., 2012; Takeshita et al., 2014; Whicher and MacKinnon, 2016; Tao and MacKinnon, 2019) and the isolated sensor of the voltage-dependent enzyme (Li et al., 2014a). Further, it has been shown that VSDs can behave as portable structural and functional units (Alabi et al., 2007; Islas, 2016).

KvAP is a K_v channel from thermophilic archaebacterium *Aeropyrum pernix* (Jiang et al., 2003; Ruta et al., 2003) and has been widely studied to understand the voltage-dependent gating mechanisms of K_v channels (Jiang et al., 2003; Cuello et al., 2004; Lee et al., 2005; Ruta et al., 2005; Li et al., 2014b). KvAP provided the first high-resolution X-ray crystal structures of voltage-dependent ion channel and the isolated VSD with the help of monoclonal Fab fragments in detergent micelles (Jiang et al., 2003; Lee et al., 2005; Torbeev, 2020). Since the crystal structure of KvAP-VSD has been obtained in the absence of membrane potential, the isolated VSD of KvAP in detergent micelles is supposed to represent the activated ('Up') state. Interestingly, a cryo EM structure of KvAP with the non-domain-swapped topology of VSD has been recently reported (Tao and MacKinnon, 2019).

In voltage-sensing proteins, the voltage sensor paddle motif (S3b-S4 helix-turn-helix) is a conserved structural unit and has functional significance. For instance, this paddle motif of KvAP-VSD when transplanted to eukaryotic K_v channels can maintain the channel function (Alabi et al., 2007). Further, the S3b-S4 loop is also a target for many venom peptide toxins that modulate the gating of K_v channels (Swartz, 2007). In KvAP sensor, the S3b-S4 loop participates in protein-protein interactions with voltage sensor peptide toxin 1 (VSTX1) from spider venom Lee and MacKinnon (2004); Lau et al., (2016), as well as antibody fragments (Jiang et al., 2003; Torbeev, 2020). We have recently shown that the organization and structural dynamics of the S3b-S4 sensor loop of the isolated VSD of KvAP is significantly altered in membrane environment compared to micelles (Das et al., 2020), in which the loop partitions into the membrane interface and experience a relaxed/dynamic organization. Further, we have demonstrated that the surface charge and curvature of the membrane do not significantly affect the topology, dynamics and structural organization of the sensor loop (Das and Raghuraman, 2021).

In addition to voltage-dependent gating, KvAP also undergoes lipid-dependent gating in a voltage-independent manner (Schmidt et al., 2006; Zheng et al., 2011; Jiang, 2019). It has been shown that the phosphate headgroup of phospholipid membranes is an absolute requirement for the normal functioning of KvAP and stabilizes the 'Up' conformation of the KvAP sensor (Schmidt et al., 2006; Zheng et al., 2011). Interestingly, the presence of non-phospholipids in the membrane shifts the conformational equilibrium from activated/'Up' to resting/'Down' state of the VSD (Schmidt et al., 2006; Zheng et al., 2011; Jiang, 2019). In this work, we have monitored the effect of cholesterol, a physiologically-relevant non-phospholipid, on the organization and dynamics of the S3b-S4 loop of the paddle motif of KvAP-VSD (Fig. 1A) in membranes using environment-sensitive site-directed fluorescence approaches (Raghuraman et al., 2019; Brahma et al., 2022) and depth measurements utilizing the parallax method (Chattopadhyay and London, 1987; Brahma and Raghuraman, 2022). Our results show that the S3b-S4 loop of KvAP-VSD partitions at the shallower interfacial region in cholesterol-containing membranes compared to PC/PG membranes. Further, the dynamic nature (rotational and hydration dynamics) and conformational heterogeneity of this functionally-important loop of KvAP sensor is significantly altered by cholesterol. Overall, these results are relevant for understanding the lipid-gating mechanisms of K_v channels in membranes in general, and KvAP in particular.

2. Materials and methods

2.1. Materials

E. coli XL1-Blue strain were purchased from Agilent (Santa Clara, CA). Triton X-100, n-decyl-β-D-maltopyranoside (DM) and n-octyl-β-D-glucopyranoside (OG) were obtained from Anatrace (Maumee, OH). Protease inhibitors were obtained from GoldBio (St. Louis, MO). 1-palmitoyl-2-oleoyl-*sn*-glycero-3-phosphocholine (POPC) and 1-palmitoyl-2-oleoyl-*sn*-glycero-3-phospho-(1′-rac-glycerol) (POPG), 1,2-dioleoyl-sn-glycero-3-phosphocholine (DOPC), 1,2-dioleoyl-sn-glycero-3-phosphotempocholine (Tempo-PC), and 1-palmitoyl-2-(5-doxyl) stearoyl-

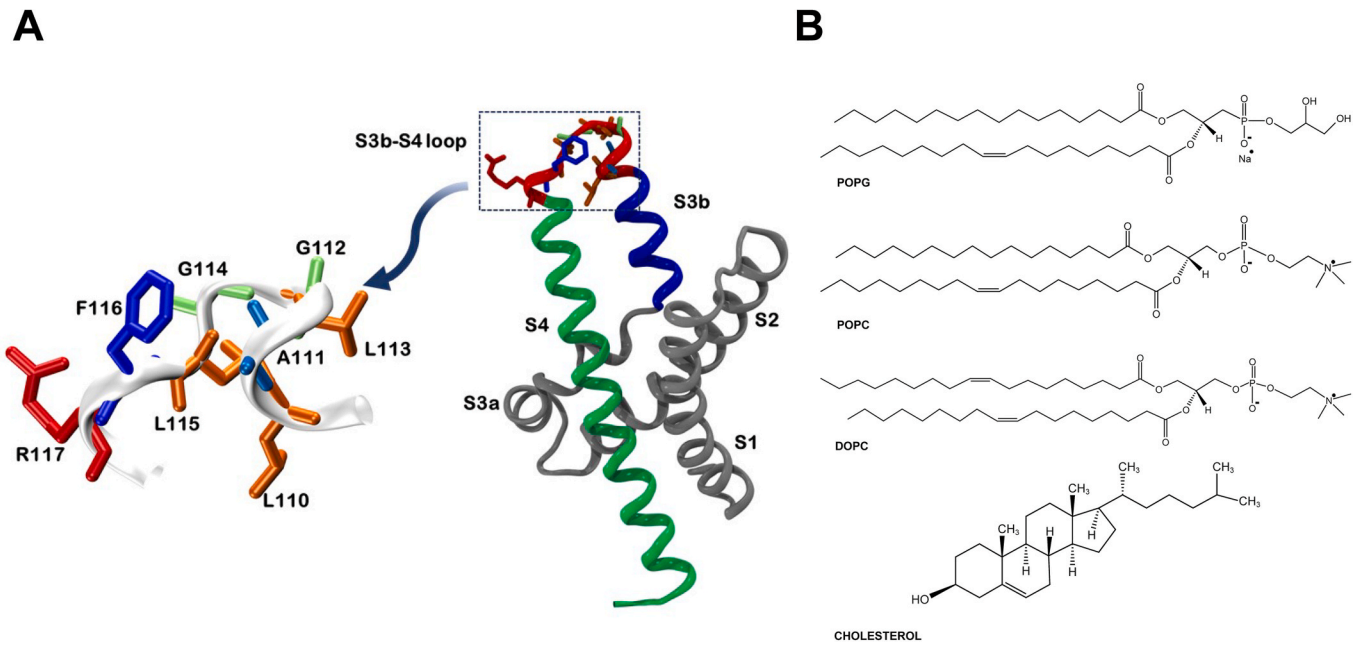

Fig. 1. The S3b-S4 loop of KvAP-VSD. (A) Cartoon representation of the isolated KvAP-VSD (PDB ID: 1ORS, chain C) is shown with its four transmembrane segments (labeled S1 to S4). The position of the S3b-S4 loop (residues 110 to 117) in the VSD is indicated by dotted box, and the native amino acid residues corresponding to this loop are shown in stick representation in enlarged view. (*B*) Shown are the chemical structures of lipids used in this study.

sn-glycero-3-phosphocholine (5-PC) were obtained from Avanti Polar Lipids (Alabaster, AL). Cholesterol, potassium iodide (KI) was purchased from Sigma Aldrich (St. Louis, MO). *N*,*N*′-dimethyl-*N*-(iodoacetyl)-*N*'-(7-nitrobenz-2-oxa-1,3-diazol-4-yl)ethylenediamine (IANBD amide) was obtained from Invitrogen (Carlsbad, CA). All other chemicals used were of the highest purity available from either Merck (Kenilworth, NJ) or Amresco (Radnor, PA).

2.2. Mutagenesis, channel expression and purification

The DNA encoding the isolated VSD of KvAP was cloned into pQE70 expression vector (Qiagen, Hilden, Germany). Single cysteine mutants were generated for residues 110 to 117, which corresponds to S3b/S4 loop of the isolated sensor. The mutations were confirmed by DNA sequencing. Single cysteine mutants of KvAP-VSD were expressed in XL1-Blue cells and purified using the dual-detergent strategy as described earlier (Das et al., 2021). The concentration of the protein was checked in a DS-11+ microvolume spectrophotometer (DeNovix, Wilmington, DE). To analyze whether the channel is folded properly, the purified protein (~17 kDa) was applied onto a Superdex 75 10/300 column (GE Healthcare, Chicago, IL) size-exclusion column equilibrated with 20 mM Tris, 100 mM KCl, 30 mM OG, pH 8.0 buffer.

3. Site-specific fluorescence labeling and membrane reconstitution

The purified single cysteine mutants of KvAP-VSD were fluorescently labeled using IANBD amide, which is a thiol-reactive environment-sensitive fluorescent probe, as described earlier (Das et al., 2020; Brahma et al., 2022). The labeled mutants of KvAP-VSD were reconstituted at a lipid-to-protein molar ratio of 100:1 in POPC:POPG (3:1, mol/mol) and cholesterol-containing (20 and 40 mol%) DOPC liposomes as described earlier (Das et al., 2020). Briefly, 480 nmoles POPC and 160 nmoles of POPG (640 nmoles of total lipids) in chloroform were mixed well and dried under a stream of nitrogen while being warmed gently (~35 °C). After the lipids were dried further under a high vacuum for at least 3 h, they were hydrated (swelled) by adding 1 ml of 20 mM Tris, 100 mM KCl, pH 8.0 buffer and vortexed vigorously for 2 min to disperse the lipids and sonicated to clarity. Protein was then added to give a molar ratio of 100:1 lipid:VSD monomer. The sample was left at room temperature for 30 min on a rotator and 200 mg of pre-washed biobeads (SM-2, Bio-Rad, Hercules, CA) were then added and the mixture was incubated on a rotator overnight at 4 °C to remove the detergent. The biobeads were removed by filtering using a Bio-Rad 5 ml column filter before use.

4. Steady-state fluorescence measurements

Steady-state fluorescence measurements were performed with a Hitachi F-7000 spectrofluorometer using 1 cm path length quartz cuvettes. Excitation and emission slits with a nominal bandpass of 5 nm were used for all measurements. Background intensities were appropriately subtracted from each sample spectrum to cancel out any contribution due to the solvent Raman peak and other scattering artifacts. Red edge excitation shift (REES) measurements were by done by measuring the emission maximum as a function of increasing excitation wavelength from 465 to 510 nm. The magnitude of REES represents the total shift in emission maximum upon the indicated change in the excitation wavelength.

Fluorescence anisotropy measurements were performed at room temperature using Hitachi polarization accessory. Anisotropy values were calculated from the equation (Brahma et al., 2022):

$$r = \frac{I_{VV} - GI_{VH}}{I_{VV} + 2GI_{VH}} \quad \text{Eq. 1}$$

where, I_{VV} and I_{VH} are the measured fluorescence intensities (after appropriate background subtraction) with the excitation polarizer vertically oriented and emission polarizer vertically and horizontally oriented, respectively. G is the grating correction factor and is the ratio of the efficiencies of the detection system for vertically and horizontally polarized light, and is equal to I_{HV}/I_{HH}. The apparent (average) rotational correlation times were calculated using Perrin's equation (Brahma et al., 2022):

$$\tau_c = < \tau > r / (r_o - r) \quad \text{Eq. 2}$$

where r_o is the limiting anisotropy of NBD, which is 0.354 (Mukherjee et al., 2004), r is the steady-state anisotropy and $<\tau>$ is the respective mean fluorescence lifetime.

5. Time-resolved fluorescence measurements

Fluorescence lifetimes were calculated from time-resolved fluorescence intensity decays using a picosecond pulsed LED-based time-correlated single-photon counting (TCSPC) fluorescence spectrometer and MCP-PMT as a detector as described earlier (Brahma et al., 2022). Lamp profiles were measured at the excitation wavelength using Ludox (colloidal silica) as the scatterer. To optimize the signal/noise ratio, 10,000 photon counts were collected in the peak channel. All experiments were performed with a bandpass of 5–8 nm. Fluorescence intensity decay curves so obtained were deconvoluted with the instrument response function and analyzed as a sum of exponential terms:

$$F(t) = \sum\nolimits_i \alpha_i \exp(-t / \tau_i) \quad \text{Eq. 3}$$

where $F(t)$ is the fluorescence intensity at time t and α_i is a pre-exponential factor representing the fractional contribution to the time-resolved decay of the component with a lifetime τ_i such that $\Sigma_i\, \alpha_i = 1$. Intensity-weighted mean (average) lifetimes $<\tau>$ for triexponential decays of fluorescence were calculated from the decay times and pre-exponential factors using the following equation (Brahma et al., 2022):

$$< \tau > = \frac{\alpha_1 {\tau_1}^2 + \alpha_2 {\tau_2}^2 + \alpha_3 {\tau_3}^2}{\alpha_1 \tau_1 + \alpha_2 \tau_2 + \alpha_3 \tau_3} \quad \text{Eq. 4}$$

The fluorescence decay data analysis by maximum entropy method (MEM) was carried out as described in detail previously (Smith et al., 2017; Brahma et al., 2022). All MEM fits were performed on a standard PC using the open access AnalyseDistribution MATLAB code [see Smith et al., 2017 for further details].

6. Fluorescence quenching measurements

Collisional quenching experiments of NBD fluorescence of proteoliposomes were carried out by measurement of fluorescence intensity of the KvAP-VSD loop residues after serial addition of small aliquots of a freshly prepared stock solution of 2.5 M potassium iodide (KI) with 1 mM $Na_2S_2O_3$ in water to a stirred sample followed by incubation for 2 min in the sample compartment in the dark (shutters closed). The excitation wavelength used was 465 nm and emission was monitored at respective emission wavelengths. The fluorescence intensities were corrected for dilution. Corrections for inner filter effect were made using the following equation (Brahma et al., 2022):

$$F = F_{obs}\ \text{antilog}[(A_{ex} + A_{em}) / 2] \quad \text{Eq. 5}$$

where F is the corrected fluorescence intensity and F_{obs} is the background subtracted fluorescence intensity of the sample. A_{ex} and A_{em} are the measured absorbance at the excitation and emission wavelengths, respectively. The absorbance of the samples was measured using a Jasco V-650 UV–visible absorption spectrophotometer. Quenching data were analyzed by fitting to the Stern- Volmer equation (Brahma et al., 2022):

$$F_o / F = 1 + K_{SV}[Q] = 1 + k_q \tau_o\, [Q] \quad \text{Eq. 6}$$

where F_o and F are the fluorescence intensities in the absence and presence of the quencher, respectively, K_{SV} is the Stern-Volmer quenching constant, and [Q] is the molar quencher concentration. The Stern-Volmer quenching constant K_{SV} is equal to $k_q\tau_o$, where k_q is the bimolecular quenching constant and τ_o is the lifetime of the fluorophore in the absence of quencher.

7. Depth measurements using the parallax method

For depth measurements of the NBD-labled mutants of KvAP sensor loop in POPC/POPG, DOPC/20 mol% cholesterol and DOPC/40 mol% cholesterol membranes, 160 nmol of total lipid was used containing 10 mol % spin-labeled phospholipid (Tempo- or 5-PC). The purified labeled protein was added to the preformed lipid vesicles at 100:1 lipid/KvAP-VSD and rotated at room temperate for 30 min followed by addition of 200 mg of prewashed biobeads to remove detergents and incubated overnight on a rotator at 4 °C. The biobeads were removed by filtering using a Bio-Rad 5 ml column filter before use. The lipid composition of these samples was as follows: i) POPC/POPG (3:1 mol/mol) (90%) and Tempo- (or 5)-PC (10%), ii) DOPC (70%), cholesterol (20%) and Tempo- (or 5)-PC (10%), and iii) DOPC (50%), cholesterol (40%) and Tempo- (or 5)-PC (10%). Triplicate samples were prepared in each case. Background samples lacking the fluorophore (KvAP-VSD) were prepared in all experiments, and their fluorescence intensity was subtracted from the respective sample fluorescence intensity. Samples were kept in the dark for 1 h before measuring fluorescence. Depths of the NBD-labeled sensor loop residues were calculated by the parallax method using the equation (Chattopadhyay and London, 1987):

$$Z_{cF} = L_{c1} + \{[(-1/\pi C)\ \ln(F_1/F_2) - L_{21}^2]/2L_{21}\} \quad \text{Eq. 7}$$

where Z_{cF} the depth of the fluorophore from the centre of the bilayer, L_{c1} the distance of the center of the bilayer from the shallow quencher (Tempo-PC in this case), L_{21} the difference in depth between the two quenchers *(i.e.*, the transverse distance between the shallow and the deep quencher), and C the two-dimensional quencher concentration in the plane of the membrane (molecules/Å^2). Here F_1/F_2 is the ratio of F_1/F_o and F_2/F_o in which F_1 and F_2 are fluorescence intensities in the presence of the shallow (Tempo-PC) and deep quencher (5-PC), respectively, both at the same quencher concentration C; F_o is the fluorescence intensity in the absence of any quencher. In membranes containing cholesterol, corrections were made for the altered concentration of spin-labeled lipids (for lateral distribution) and the depths of the quenchers used as described previously (Kaiser and London, 1998).

3. Results

The effect of membrane cholesterol on the organization and dynamics of the S3b-S4 loop residues (110–117) of the paddle motif of the isolated VSD of KvAP (Fig. 1A) utilizing the site-directed NBD fluorescence is the focus of this work. As mentioned earlier, while phospholipids like POPC/POPG stabilize the 'Up' conformation of the sensor, the presence of non-phospholipids like cholesterol has been shown to inhibit the channel activity by stabilizing the 'Down' conformation of the VSD (Zheng et al., 2011; Jiang, 2019). Fig. 1B shows the chemical structures of the lipids used in this study. We have previously shown that the structural integrity of KvAP-VSD is preserved upon NBD labeling, and therefore could be used to monitor the structural dynamics of the S3b-S4 loop residues in membrane-mimetic systems (Das et al., 2020; Das and Raghuraman, 2021).

3.1. Probe environment of sensor loop residues in cholesterol-containing membranes

It is well established that NBD exhibits a high degree of environmental sensitivity, *i.e.*, it is weakly fluorescent in water and fluoresces brightly in the visible range upon transfer to a hydrophobic medium (Fery-Forgues et al., 1993; Raghuraman et al., 2019). This property of NBD has been widely used to monitor the dynamics of membranes (Mukherjee et al., 2004; Raghuraman et al., 2007), and various classes of membrane peptides/proteins (Crowley et al., 1993; Shepard et al., 1998; Johnson, 2005; Raghuraman and Chattopadhyay, 2007; Raghuraman et al. 2014, 2019; Das et al., 2020; Das and Raghuraman, 2021).

Fig. 2A shows the representative emission scans of NBD-labeled G112C in PC/PG and cholesterol-containing DOPC membranes to highlight the differences in probe environment induced by cholesterol. The fluorescence emission maximum of 112-NBD is 538 nm in PC/PG membranes and is red shifted to ~540 nm in DOPC/cholesterol membranes (Fig. 2B), which is accompanied by a significant reduction (~50–60%) in the fluorescence intensity of NBD. This suggests that the microenvironment experienced by this residue is different in membranes containing cholesterol. Similar red-shifted emission maximum of NBD is observed in residues 110, 114, 115, and 117 residues of the sensor loop. The emission maximum profile for the entire sensor loop residues is quite similar in both PC/PG and DOPC/cholesterol membranes (Fig. 2B), which suggests that the S3b-S4 loop is located at the membrane interfacial region and experiences heterogeneous environment in both cases. Interestingly, the fluorescence intensity of NBD group in all the S3b-S4 loop residues is significantly reduced (~20–70%) in the presence of cholesterol (Fig. 2C), suggesting a significant increase in the polarity of the microenvironment around the sensor loop possibly due to both specific and general bilayer effects induced by cholesterol.

While the fluorescence emission intensity changes may not always be reliable due to its composite property that is dependent on several factors (Shepard et al., 1998; Datta et al., 2020), fluorescence lifetime is an intrinsic property of the probe and serves as a faithful indicator of the local environment (Berezin and Achilefu, 2010). We, therefore, measured fluorescence lifetimes of NBD-labeled sensor loop residues using time-correlated single photon counting (TCSPC) method. The fluorescence lifetime of NBD group is known to be sensitive to its environmental polarity (Lin and Struve, 1991; Chattopadhyay et al., 2002), the magnitude of lifetime can directly reveal the environment of the probe and in particular its exposure to water (Raghuraman and Chattopadhyay, 2007; Das and Raghuraman, 2021). For instance, the fluorescence lifetimes of NBD in membranes are in the range of ~5–10 ns (Mukherjee et al., 2004; Raghuraman et al., 2007; Raghuraman and Chattopadhyay, 2007), however, it dramatically decreases to <1 ns upon complete exposure to aqueous medium. Particularly, the free IANBD dye exhibits a sub-nanosecond lifetime of 0.58 ns in buffer (Das and Raghuraman, 2021). Typical decay profiles of 112-NBD in PC/PG membranes and DOPC membranes containing 20 and 40 mol% cholesterol with its tri-exponential fitting and the statistical parameters to check the goodness of fit are shown in Fig. 3A. The intensity-weighted mean fluorescence lifetimes, $<\tau>$, of NBD-labeled loop residues in all membranes are shown in Fig. 3B. With respect to PC/PG membranes, where the sensor assumes the 'Up' conformation, the fluorescence lifetime of NBD for residues 110 to 114 decreases substantially (~20%) in cholesterol-containing membranes, which is consistent with our earlier observation of decreased fluorescence intensity for these residues. Interestingly, the loop residues 115 to 117 exhibit the opposite trend in the sense that the presence of cholesterol increase the lifetimes compared to PC/PG membranes (Fig. 3C). This significant changes in lifetimes of NBD-labeled sensor loop is dependent on the concentration of cholesterol in DOPC membranes. These results suggest that the loop is localized in environments of heterogeneous polarity in cholesterol-containing membranes, which might arise due to the cholesterol-induced hydration changes in the membrane or the change in the conformation of the sensor (*i.e.*, 'Down' state), or a combination of both. We believe the latter might be the predominant factor in this case due to the following: Although it is known that cholesterol increases the water penetration at the membrane interface (Subczynski et al., 1994), and increased water content is known to dramatically decrease the NBD

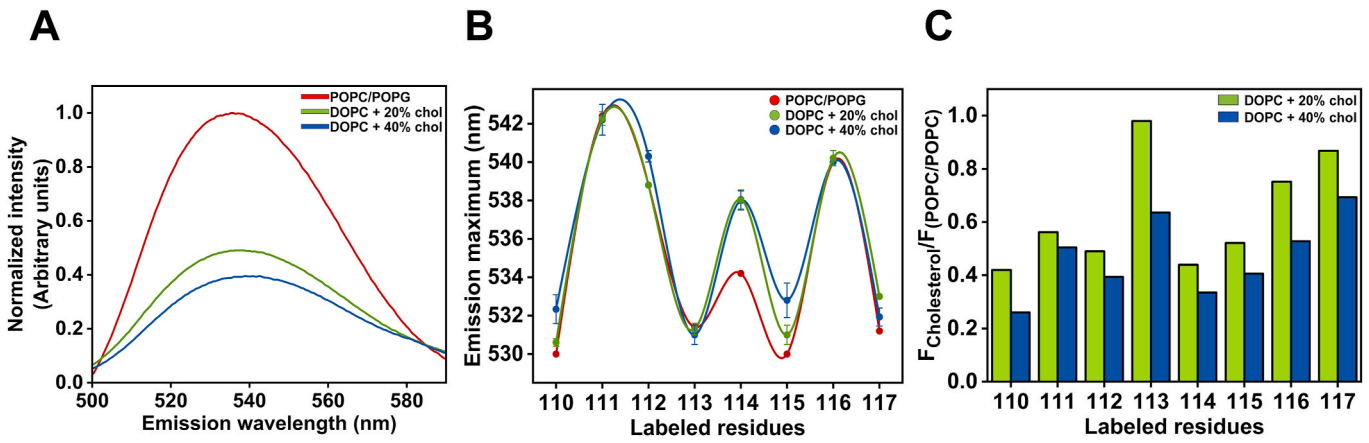

Fig. 2. Fluorescence emission of the NBD-labeled S3b-S4 loop residues in various membranes. (*A*) Representative fluorescence emission spectra of G112-NBD (solid line) in POPC/POPG (3:1 mol/mol) membranes (red), DOPC membranes containing 20 mol% (green) and 40 mol% (blue) cholesterol are shown. (*B*) Shown are the fluorescence emission maximum of NBD-labeled S3b-S4 loop residues in POPC/POPG (red) and in DOPC/20% (green) and DOPC/40% (blue) cholesterol-containing membranes. The lines joining the data points are provided merely as viewing guides. Data shown for PC/PG membranes are adapted from Das et al., (2020) for comparison. Values represent mean ± SE of three independent measurements for cholesterol-containing DOPC membranes. (C) Relative normalized emission intensity of NBD-labeled loop residues in DOPC/20 mol% cholesterol (green) and DOPC/40 mol% cholesterol (blue) with respect to PC/PG membranes is shown. The excitation wavelength used was 465 nm and emission was monitored at respective emission maximum. The protein-to-lipid molar ratio was 1:100, and the concentration of KvAP-VSD used was 3.2 μM in all cases. See Materials and Methods for details. (For interpretation of the references to colour in this figure legend, the reader is referred to the Web version of this article.)

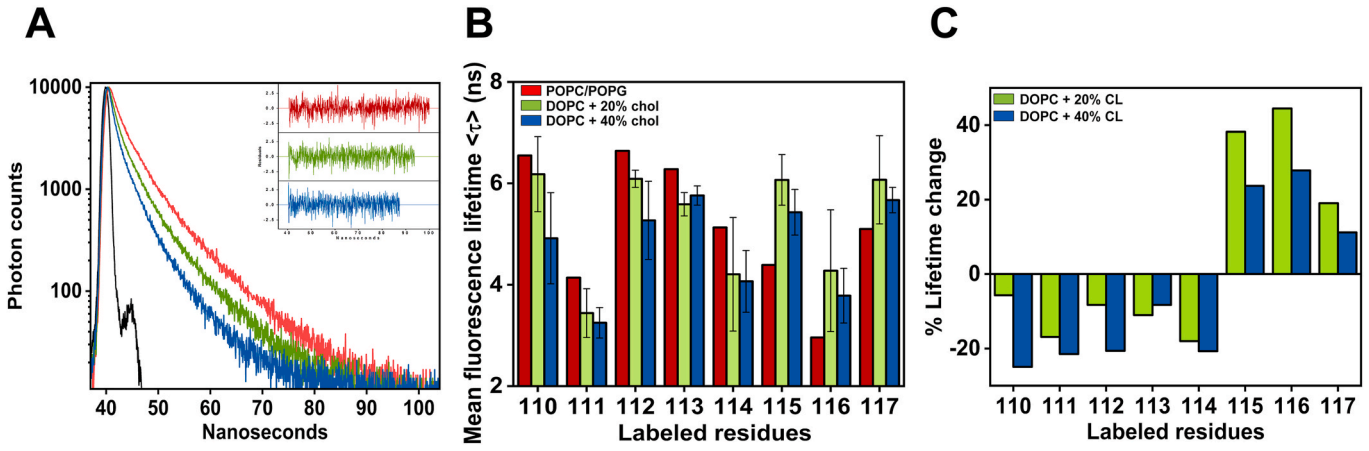

Fig. 3. Time-resolved fluorescence of NBD-labeled loop residues. (A) Time-resolved fluorescence intensity decay of G112-NBD in PC/PG membranes (red), DOPC/20 mol% cholesterol (green) and DOPC/40 mol% cholesterol (blue) is shown. Excitation wavelength was 465 nm, and emission monitored at respective emission maximum. The sharp peak on the left (black) is the lamp profile, and the relatively broad peak on the right is the decay profile (coloured lines), fitted to a triexponential function. The plot in the inset shows the weighted residuals of the decay fit. (B) Mean fluorescence lifetimes (mean ± SE of three independent measurements) of the NBD-labeled loop in different membranes, and (C) changes in lifetime for NBD-labeled loop in cholesterol-containing membranes with respect to PC/PG membranes are shown. Data shown for PC/PG membranes are adapted from Das et al., (2020) for comparison. All other conditions and colour for samples are as in Fig. 2. See Materials and Methods for other details. (For interpretation of the references to colour in this figure legend, the reader is referred to the Web version of this article.)

lifetime (Chattopadhyay et al., 2002), we would have observed a reduction in lifetimes for all the residues of the sensor loop, which is not the case (see Fig. 3C). Further, the sensor loop residues are very well shielded from the water accessibility in both PC/PG and DOPC/cholesterol membranes (see below).

3.2. *Water accessibility of sensor loop residues in cholesterol-containing membranes*

To understand the nature of sensor's loop location in cholesterol-containing membranes, we probed water accessibility using collisional quenching of NBD fluorescence by employing the widely used potassium iodide (KI) as the aqueous quencher (Crowley et al., 1993; Chatterjee et al., 2021; Brahma et al., 2022). Fig. 4A shows the representative results for quenching of 116-NBD in PC/PG and in DOPC membranes containing different concentration of cholesterol as Stern-Volmer plots. The slope of such a plot (K_{SV}), which is related to the degree of exposure of the NBD group to water, for sensor loop residues is shown in Fig. 4C. The K_{SV} values suggest that quenching by iodide ions for most of the loop residues follow a similar trend irrespective of the presence of cholesterol. Since the K_{SV} values are intrinsically dependent on the fluorescence lifetime (see Eq. (5)), we calculated the bimolecular quenching constant (k_q), which takes into account the differences in lifetimes and, therefore, offers more precise information on the degree of water exposure. Although the calculated k_q values (Fig. 4D) for the NBD-labeled loop residues follow similar trend in both PC/PG and DOPC/40% cholesterol membranes, interestingly, the residues 111 and 116 show decreased water accessibility in presence of cholesterol.

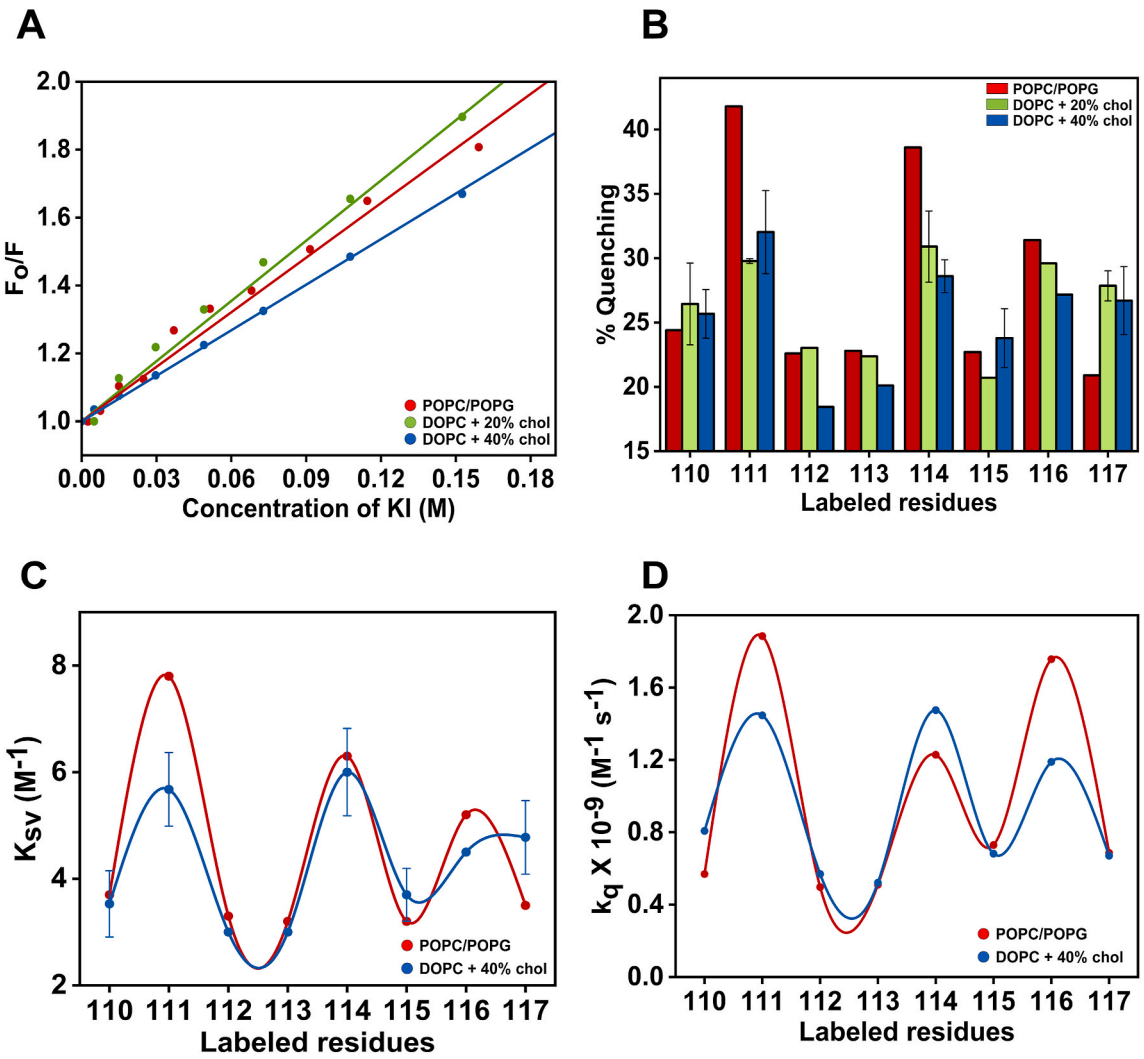

Fig. 4. Water accessibility probed by iodide quenching of NBD fluorescence. (A) Representative data of Stern-Volmer analysis of KI quenching in PC/PG liposomes (red), DOPC/20 mol% cholesterol (green) and DOPC/40 mol% cholesterol (blue) for F116-NBD of KvAP-VSD are shown. F_o is the fluorescence intensity in absence of quencher, F is the corrected fluorescence intensity in the presence of quencher. The excitation wavelength was 465 nm and emission was monitored at respective emission maximum. (B) Quenching of NBD fluorescence of the labeled loop residues at 0.1 M KI in PC/PG (red) and 20 mol% (green) and 40 mol% (blue) containing DOPC. Shown are (C) Stern-Volmer constants (K_{sv}) and (D) bimolecular quenching constants (k_q) for iodide quenching of NBD-labeled residues in PC/PG (red) and DOPC/40 mol% (blue) membranes. The lines joining the data points are provided merely as viewing guides. Data shown for PC/PG membranes are adapted from Das et al., (2020) for comparison. All other conditions are as in Fig. 2. See Materials and Methods for other details. (For interpretation of the references to colour in this figure legend, the reader is referred to the Web version of this article.)

Further, considering the k_q value of ~8 M^{-1} ns^{-1} for the complete exposure of NBD to aqueous medium (Crowley et al., 1993; Brahma et al., 2022), the calculated k_q values of ~0.5–2 M^{-1} ns^{-1} in both membranes suggest that the loop residues are well shielded from the exposure to water, which is in agreement with lifetime measurements. This clearly suggests that the significant reduction in the fluorescence intensity of NBD-labeled sensor loop observed (see Fig. 2C) was not due to increased water penetration at the interfacial region of the membrane. If cholesterol-induced increase in hydration at the membrane interface is only considered, we would have seen an increase in water accessibility for all the loop residues. The fact that the quenching profiles show similar trend in both PC/PG and DOPC/cholesterol membranes (Fig. 4D), and the water accessibility is reduced for residues 111 and 116 suggests that the indirect effect of cholesterol-induced changes in bulk bilayer properties may not be the predominant factor and supports the conformational changes of the voltage sensor to the 'Down' state in cholesterol-containing membranes (Zheng et al., 2011; Jiang, 2019).

3.3. Hydration dynamics around the sensor loop residues in cholesterol-containing membranes

It is well known that protein dynamics is intrinsically related to hydrating solvent molecules and slow solvation (Li et al., 2007; Bellissent-Funel et al., 2016). Further, hydration dynamics have been shown to play crucial roles in lipid-protein interactions (Raghuraman and Chattopadhyay, 2007; Das et al., 2020; Chatterjee et al., 2021) mediating ion channel functional states (Raghuraman et al., 2014) and ion channel selectivity (Roux, 2017). Red edge excitation shift (REES) is a well-established fluorescence approach, which provides novel insights on the relative rates of water relaxation dynamics in complex biological systems and is sensitive to changes in local hydration dynamics (Demchenko, 2008; Brahma and Raghuraman, 2021). Further, the sensitivity of REES to changes in local hydration dynamics has been widely used as a powerful tool to probe the presence of restricted/bound water molecules, side-chain rearrangements in a protein core and protein conformational substates (see Brahma and Raghuraman, 2021 for a review).

REES is operationally defined as the shift in the fluorescence

emission maximum towards higher wavelengths caused by a shift in the excitation wavelength towards the red edge of the absorption band. Fig. 5A shows the representative data for change in emission maximum as a function of changing excitation wavelength from 465 to 510 nm for the 112-NBD residue of the sensor loop in PC/PG and cholesterol-containing DOPC membranes. The magnitude of REES, *i.e.*, the total shift in emission maximum upon changing the excitation wavelength, is shown in Fig. 5B. In general, all the loop residues exhibit REES irrespective of the presence of cholesterol in the membrane suggesting the slow solvent relaxation and the presence of restricted water molecules in the ns time scale (Brahma and Raghuraman, 2021). Interestingly, the voltage sensor loop undergoes differential hydration dynamics in the presence of cholesterol since the magnitude of REES increases for most of the residues from 110 to 115, and it decreases for the residues 116 and 117 that are close to the S4 helix. This pattern, *i.e.*, the two halves of the sensor loop showing differential behaviour, somewhat resembles the changes in lifetimes in the presence of cholesterol (see Fig. 2C). This clearly indicates that the environmental restriction, which is offered by the relaxing water molecules, around the loop residues is significantly altered by cholesterol. It should be noted that we have shown previously that the residue 115 does not exhibit REES in PC/PG membranes (Das et al., 2020), but exhibits a modest REES of 1 nm in the presence of cholesterol. As shown earlier, the overall water accessibility remains similar in PC/PG and DOPC/cholesterol membranes (Fig. 4D) and the REES results are therefore not due to the change in the hydration status of the membrane. This can only be attributed to the change in the voltage sensor loop conformation in cholesterol-containing membranes.

3.4. Rotational dynamics of the KvAP-VSD loop residues in cholesterol-containing membranes

Fluorescence anisotropy is a powerful approach to obtain information about the molecular flexibility and rotational motion of a fluorophore (James and Jameson, 2014) and has been used to monitor the dynamic behaviour of ion channels (Ho et al., 2013; Raghuraman et al., 2014; Chatterjee et al., 2021; Brahma et al., 2022). It is well known that the rapidly tumbling NBD displays negligible anisotropy, whereas its limiting anisotropy is 0.354 (Mukherjee et al., 2004; Brahma et al., 2022). We measured the steady-state fluorescence anisotropy values of NBD-labeled S3b-S4 loop residues in PC/PG and DOPC/cholesterol membranes, which is in the range of ~0.17–0.26 (Fig. 6A). This, in general, indicates that the rotational mobility of the NBD-labeled sensor loop is considerably restricted and are representative of motionally-restricted environments of NBD. This is in agreement with REES results and suggest the localization of the sensor loop at the membrane interfacial region.

We have recently shown that both POPC and POPC/POPG membrane environments offer a similar dynamic (relaxed) organization of the VSD sensor loop with significant dynamic variability, which rules out the membrane surface charge effects on the dynamic organization of the VSD sensor loop (Das et al., 2020; Das and Raghuraman, 2021). Compared to PC/PG membranes, the addition of 20 mol% cholesterol not only changes the anisotropy values in a segmental fashion but also changes the periodic pattern of the dynamic variability (Fig. 6A). Interestingly, the anisotropy values for the S3b-S4 loop residues are significantly reduced upon addition of 40 mol% cholesterol, suggesting that high concentration of cholesterol makes the sensor loop more dynamic in nature. Further, the dynamic variability exhibited by the sensor loop in PC/PG and DOPC/20% cholesterol membranes is lost at high concentration of cholesterol (Fig. 6A). This could be due to the change in the lipid packing in membranes due to the formation of liquid-ordered (lo) phase at high concentration of cholesterol (de Meyer and Smit, 2009; Marsh, 2010; Heberle and Feigenson, 2011).

As discussed above, the lifetime changes are more pronounced especially for the loop residues in membranes containing cholesterol. To ensure that the anisotropy values measured for the NBD-labeled loop residues of KvAP-VSD do not suffer from lifetime-induced artifacts, apparent rotational correlation times were calculated and are shown in Fig. 6B. As can be seen from the figure, the rotational correlation times (τ_c), on average, for the loop residues of the sensor in both PC/PG and DOPC/20% cholesterol membranes is 7–15 ns, highlighting that the S3b-S4 loop region of the sensor exhibits high dynamic variability in these membranes, consistent with the EPR results (Chakrapani et al., 2008). In the presence of 40 mol% cholesterol in membranes, the corresponding τ_c values for the loop residues have significantly reduced and is in the range of 5–10 ns. Comparing the τ_c values of the sensor loop in PC/PG membranes (stabilizes the 'Up' state of the VSD) and cholesterol-containing membranes (stabilizes the 'Down' state), it is clear that the loop residues 110 to 114, in general, is highly dynamic at high concentration of cholesterol, although residues 110 to 112 behave

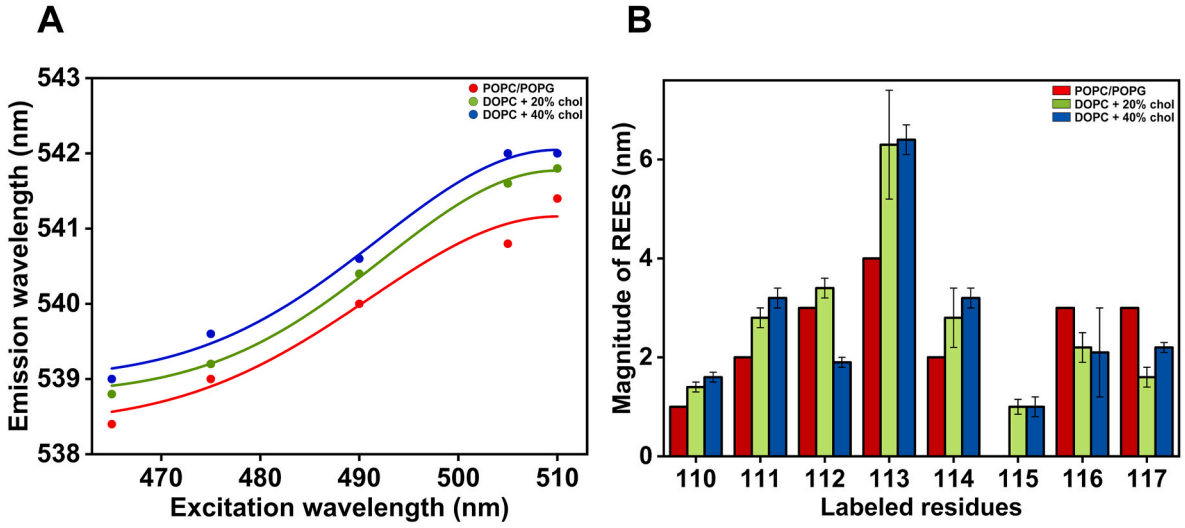

Fig. 5. Hydration dynamics of NBD-labeled loop residues in cholesterol-containing membranes (A) REES measurements of the effect of changing excitation wavelength on the wavelength of emission maximum for G112-NBD in PC/PG liposomes (red), DOPC/20 mol% cholesterol (green) and DOPC/40 mol% cholesterol (blue) is shown along with (B) the magnitude of REES for the S3b-S4 loop residues. Data shown for PC/PG membranes are adapted from Das et al., (2020) for comparison. The lines joining the data points are provided merely as viewing guides. All other conditions are as in Fig. 2. See Materials and Methods for details. (For interpretation of the references to colour in this figure legend, the reader is referred to the Web version of this article.)

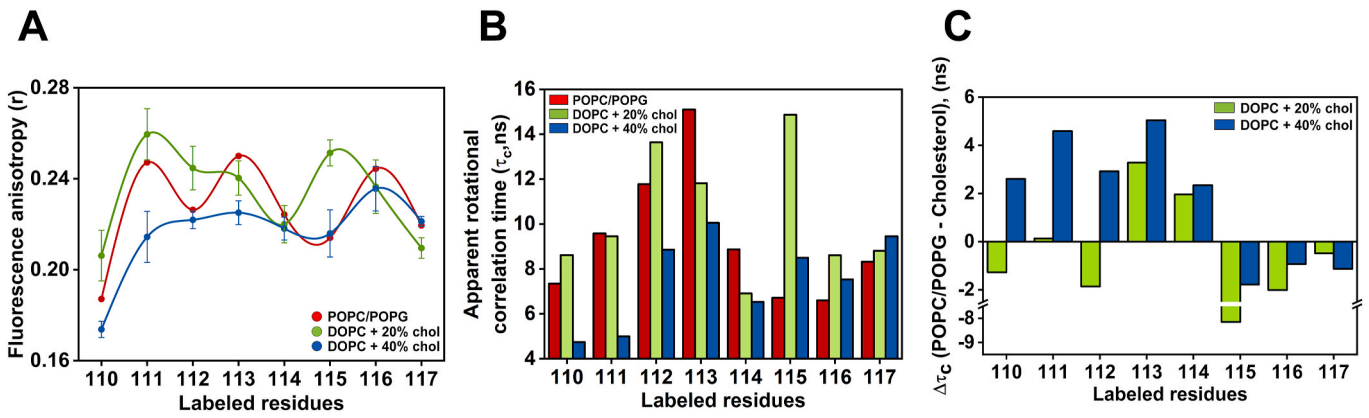

Fig. 6. Modulation of rotational mobility of S3b-S4 loop residues of KvAP-VSD by cholesterol. Steady-state fluorescence anisotropy measurements of NBD fluorescence (A) and the calculated apparent rotational correlation times (τ_c) of the NBD-labeled S3b-S4 loop residues (B) in PC/PG liposomes (red), DOPC/20 mol% cholesterol (green) and DOPC/40 mol% cholesterol (blue). The lines joining the data points are provided merely as viewing guides. (C) The effect of cholesterol concentration on τ_c of loop residues with respect to PC/PG membranes is shown as $\Delta\tau_c$, The error bars represent mean ± S.E. of three independent measurements. Data shown for PC/PG membranes are adapted from Das et al., (2020) for comparison. All other conditions are as in Fig. 2. See Materials and Methods for other details. (For interpretation of the references to colour in this figure legend, the reader is referred to the Web version of this article.)

differently in membranes containing 20% cholesterol. However, residues 115 to 117 experience a restricted mobility in the presence of high concentration of cholesterol, and, this motional restriction of these residues are correlated well with the corresponding increase in lifetimes in cholesterol-containing membranes (see Fig. 3C). Taken together, our results clearly suggest that cholesterol modulates the rotational dynamics (mobility) of the voltage sensor loop depending on its concentration in membranes.

3.5. *Membrane penetration depths of the KvAP-VSD loop residues*

Membrane penetration depth represents an important parameter in the study of the structure and organization of membranes and membrane proteins (London and Ladokhin, 2002; Brahma and Raghuraman, 2022). Further, fluorescence quenching-based distance measurements have been widely utilized to get crucial insights on the conformational changes in membrane peptides/proteins, particularly for the NBD-labeled ones (Raghuraman and Chattopadhyay, 2007; Bradberry et al., 2019; Kyrychenko et al., 2022; Brahma and Raghuraman, 2022). To gain a better understanding of the cholesterol-induced change in the organization and conformation of the S3b-S4 voltage sensor loop in membranes, we measured the 'average' membrane penetration depths of the NBD group for some of the NBD-labeled sensor loop residues using the parallax method (see London and Ladokhin, 2002; Brahma and Raghuraman, 2022 for reviews). Representative quenching of NBD fluorescence of 110-NBD by nitroxide quenchers Tempo-PC and 5-PC is shown in Fig. 7A. The measured distances for the NBD-labeled sensor loop residues 110, 113, 114 and 116 in PC/PG and DOPC/cholesterol membranes are shown in Fig. 7B. The distance measurements from the center of the bilayer suggests that irrespective of the lipid composition

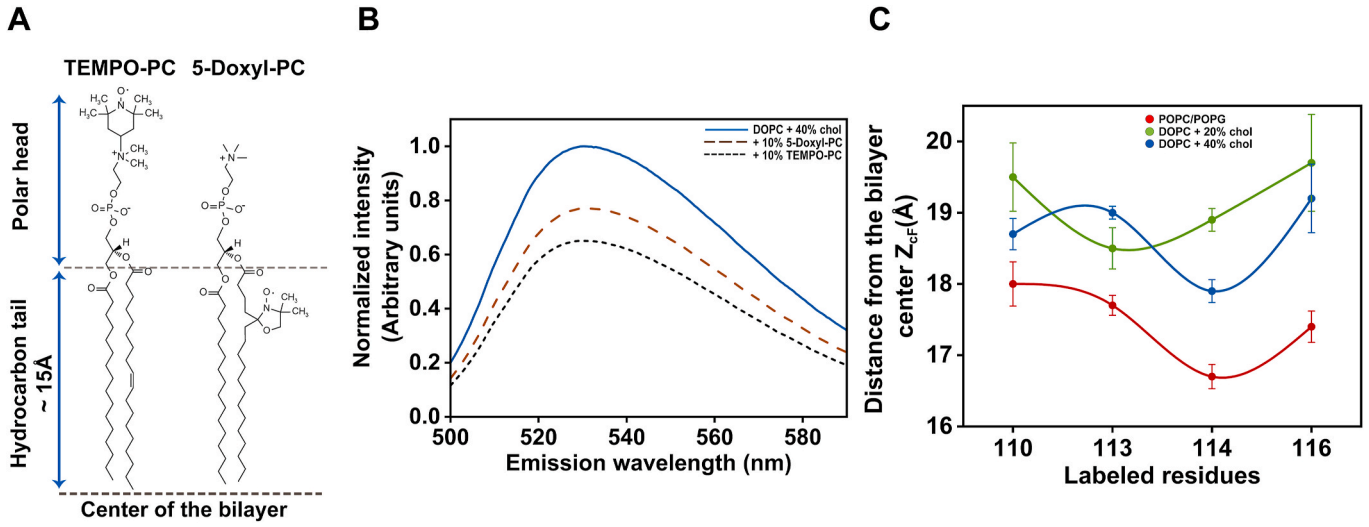

Fig. 7. Measurement of membrane penetration depths of NBD-labeled S3b-S4 loop residues by parallax method. (A) The chemical structures of TEMPO-PC and 5-doxyl-PC and their positions from the center of the bilayer is shown. (B) Representative fluorescence emission spectra of L110-NBD in DOPC/40% cholesterol membranes in the absence (blue) and in the presence of nitroxide quencher Tempo-PC (dashed line) and 5-doxyl PC (dotted line) are shown. (C) The average distance measured for the indicated NBD-labeled loop residues from the bilayer center in POPC/POPG (red) and DOPC membranes containing 20% (green) and 40% (blue) cholesterol is shown. The protein-to-lipid molar ratio was 1:100, and the concentration of KvAP-VSD used was 1.6 μM in all cases. The excitation wavelength was 465 nm and the intensity was monitored at respective emission maximum. The values represent mean ± SE of three independent measurements. Corrections were made for the altered concentrations of spin-labeled lipids (for lateral distribution) and the depths of the quenchers used in membranes containing cholesterol See Materials and Methods for details. (For interpretation of the references to colour in this figure legend, the reader is referred to the Web version of this article.)

used, the NBD group of the NBD-labeled sensor loop is located ~17–20 Å (near headgroups) from the center of the membrane bilayer, suggesting that the KvAP-VSD loop resides at the membrane interfacial region irrespective of the presence or absence of cholesterol and the associated functional states. While in PC/PG membranes, the sensor loop is, on average, localized at ~17–18 A from the bilayer center, there is a decrease in membrane penetration depth (~2 Å) for the loop residues in cholesterol-containing membranes (Fig. 7B). This suggests that the sensor loop is positioned at relatively shallow membrane interfacial region of the membranes that contain cholesterol. This decreased membrane penetration depth in cholesterol-containing membranes is similar to what was observed with interfacially-localised hemolytic peptide melittin (Raghuraman and Chattopadhyay, 2007). Interestingly, the depth values obtained at 40% cholesterol are slightly lower than the corresponding values obtained at 20% cholesterol containing membranes in most cases. Overall, our results demonstrate the altered organization of the sensor loop in cholesterol-containing membranes.

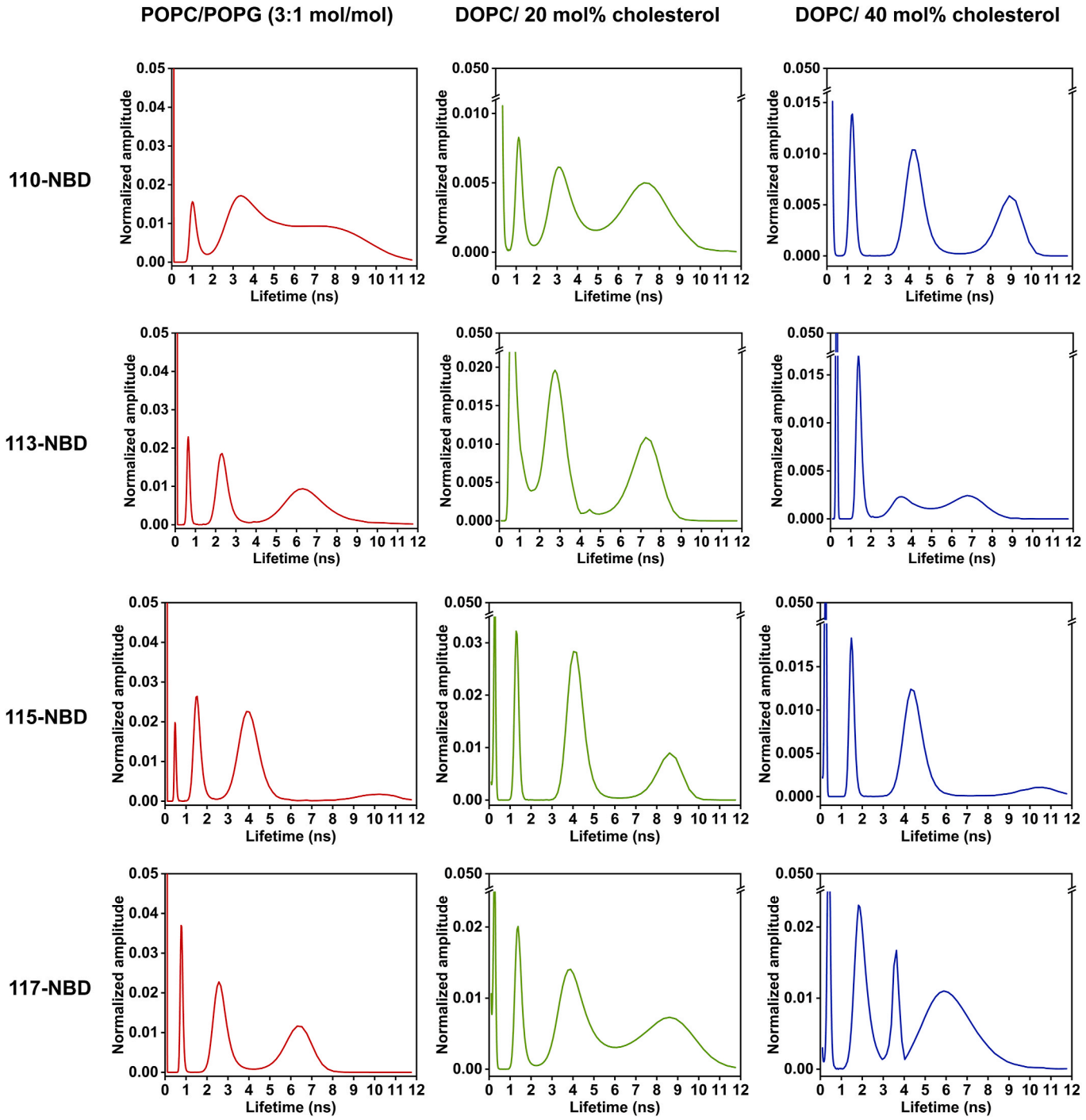

Fig. 8. Conformational heterogeneity of KvAP sensor loop in cholesterol-containing membranes. MEM fluorescence lifetime distributions for the NBD-labeled sensor loop residues 110, 113, 115, 117 in PC/PG, DOPC/20% and DOPC/40% cholesterol containing membranes are shown. The normalized probability amplitudes are plotted against their corresponding lifetime on a linear scale. All other conditions are as in Fig. 2. See Materials and Methods for details.

3.6. Conformational heterogeneity of the KvAP-VSD loop in cholesterol-containing membranes

While fluorescence lifetime of NBD serves as a faithful indicator of its local environment, its emission decay kinetics gives information about the structural heterogeneity when incorporated in a complex system (Brahma et al., 2022). Importantly, fluorescence lifetime distribution gives an ultrafast snapshot of the protein population distribution (Krishnamoorthy, 2018). Particularly, Maximum Entropy Method (MEM) analysis of fluorescence decay involves resolving the lifetime components in a model-independent manner (Smith et al., 2017; Brahma et al., 2022). MEM has been widely used to monitor the unfolding transitions and conformational heterogeneity in several soluble proteins, and to monitor membrane heterogeneity (Krishnamoorthy, 2018; Raghuraman et al., 2019). This powerful MEM approach has recently been utilized in deciphering conformational heterogeneity of membrane proteins like KvAP voltage sensor (Das and Raghuraman, 2021) and MgtE homologs (Chatterjee et al., 2021; Brahma and Raghuraman, 2024).

Representative MEM lifetime distribution profiles for the VSD loop residues 110, 113, 115 and 117 in PC/PG membranes and DOPC membranes containing varying amounts of cholesterol are shown in Fig. 8. In general, the number of peaks in the probability distribution profile is interpreted as the number of discrete conformations of the fluorophore, the peak areas reflect their relative populations and the width is used to interpret the heterogeneity (Smith et al., 2017; Krishnamoorthy, 2018; Brahma et al., 2022). Irrespective of the membrane system used, the fluorescence lifetime distribution profiles for the indicated NBD-labeled sensor loop residues contain multiple peaks and are complex, which is not surprising considering the complex nature of organized molecular assemblies like ion channels. Monitoring the changes in conformational heterogeneity in different functional states of the KvAP-VSD S3b-S4 loop is, therefore, not trivial. However, changes in lifetime distribution profiles might offer significant insights into the nature of altered conformational substates. Since fully-exposed NBD in aqueous solution has a sub-nanosecond lifetime (Das and Raghuraman, 2021) and the lifetimes can increase dramatically in hydrophobic environments (Lin and Struve, 1991; Fery-Forgues et al., 1993; Raghuraman et al., 2019), the lifetimes in the range of 1–10 ns can be considered to understand the change in conformational heterogeneity, if any, induced by cholesterol. In PC/PG membranes, the 110-NBD residue of the loop shows a heterogeneous distribution of lifetimes in such a way that the lifetime distribution is spread from 2 to 10 ns. Interestingly, this same residue shows three discrete peaks in cholesterol-containing membranes (Fig. 8). Further, NBD-labeled residues 113, 115 and 117 has two peaks in PC/PG membranes between 1 and 10 ns, but the presence of cholesterol in membranes changes the lifetime distribution width and number of peaks in most cases, particularly for the first gating charge residue 117. This clearly indicates that sensor loop undergoes significant changes in conformational heterogeneity in membranes containing cholesterol, which could be due to the change in location of the sensor loop within the membrane interface (see Fig. 7B) caused by the change in conformation of the KvAP-VSD to 'Down' state (Zheng et al., 2011; Jiang, 2019).

4. Discussion

Lipid-protein interactions are crucial for the organization and function of biological membranes, and are involved in plethora of important cellular functions that include organizing functional membrane domains, regulation of transmembrane ion transport, signal transduction, host-pathogen interactions (Lee, 2003, 2004, 2011; Rao and Mayor, 2014; Corradi et al., 2019; Sych et al., 2022; Kusumi et al., 2023). Membrane lipids play an important role in modulating the structure and function of various membrane proteins due to their specific high-affinity binding (Hunte, 2005). The critical dependence of proteins on the chemical nature of the lipid bilayer therefore suggests that the two might have coevolved (Lee, 2004).

Cholesterol is a ubiquitous membrane component of eukaryotes. Like other membrane lipids, cholesterol is amphiphilic, yet its rigid structure differs significantly from other lipid species of eukaryotic cell membranes (Subczynski et al., 2017). It is also the most important functionally-relevant non-phospholipid in human health and disease. Due to its unique structural features, cholesterol affects the physical properties of model and biological membranes (Yeagle, 1985; Meza et al., 2020). It is quite established that the distribution of cholesterol in the cellular membranes is not uniform, rather there exists a cholesterol gradient, *i.e.*, cholesterol is present at ~35–45 mol% in the plasma membrane and is severely depleted in intracellular membranes (Yeagle, 1985; van Meer et al., 2008; Subczynski et al., 2017). Cholesterol is often laterally associated with sphingolipids in plasma membranes to form lateral membrane heterogeneities called functional microdomains or 'rafts' that have been implicated in various functions in mammalian cells (Lingwood and Simons, 2010; Rao and Mayor, 2014; Kusumi et al., 2023). Importantly, cholesterol is a major regulator of the function of different classes of membrane proteins like ion channels, transporters and G-protein coupled receptors through direct and indirect effects (Levitan et al., 2014; Zakany et al., 2020; Meza et al., 2020; Taghon et al., 2021; Yeagle, 2022). Particularly, cholesterol affects the functional activity of voltage-gated (K_v), inward rectifier K^+ (Kir), and BK channels (Levitan et al., 2014; Zakany et al., 2020).

In humans, >70 Kv channels are encoded in their genome and they are crucial for maintaining the electrical excitability of cells and also involved in chemical signalling (Gunthrope, 2022). Even subtle mutations in them leads to drastic changes in their functional behaviour and underlie many genetically-inherited pathological conditions (Catterall, 2010). Kv channels are, therefore, important drug targets (Wulff et al., 2009). The first crystal structures of the voltage-gated ion channels have been determined for the prokaryotic Kv channel, KvAP (Jiang et al., 2003; Lee et al., 2005). Further, it has been shown that local lipid composition has an influence on the topology and conformation of the voltage sensor in a voltage-independent manner (*i.e.*, lipid-dependent gating). For instance, it has been shown that lipid phosphate head groups are critical for the normal functioning of Kv channels (Schmidt et al., 2006; Ramu et al., 2006; Xu et al., 2008; Zheng et al., 2011). Indeed, non-phosphate containing lipids, including cholesterol, have been shown to stabilize the resting/'Down' conformation of the VSD in KvAP (Schmidt et al., 2006; Zheng et al., 2011; Jiang and Gonen, 2012). These studies clearly demonstrate the importance of lipid-protein interactions in membranes for the functioning of Kv channels.

The isolated VSD of KvAP has been studied as a model system to understand the structural dynamics of voltage sensor in membranes (Chakrapani et al., 2008; Li et al., 2014b; Das et al., 2020; Das and Raghuraman, 2021; Ngoc et al., 2021), and particularly the sensor movement related to lipid-dependent gating mechanism of Kv channels (Li et al., 2014b). As mentioned earlier, the KvAP-VSD is a four-helix bundle (helices S1–S4) and its basic architecture is common to other voltage-sensing proteins. The S3b-S4 loop is a functionally important region of the KvAP-VSD since the voltage sensor toxin 1 from spider venom (VSTX1) partitions into lipid membrane and interacts with G114, L115 and F116 in S3b-S4 loop (Lau et al., 2016), and inhibits KvAP (Lee and MacKinnon, 2004; Alabi et al., 2007; Lau et al., 2016). Considering that the voltage-dependent activity of KvAP was completely lost in DOPC membranes containing more than 15 mol% cholesterol that could be attributed to cholesterol-induced conformational switch to 'Down' state of the VSD (Zheng et al., 2011), understanding the structural dynamics of this important loop of the KvAP-VSD in cholesterol-containing membranes assumes significance.

We have monitored the structural dynamics of the S3b-S4 loop of KvAP-VSD in 20 and 40 mol% cholesterol-containing DOPC membranes and compared our results with POPC/POPG membranes. To the best of our knowledge, this work constitutes the first report that describes the

cholesterol-induced structural dynamics of this functionally important sensor loop of KvAP. Based on our results, we propose a model on the altered organization and dynamics of the KvAP-VSD sensor loop in cholesterol-containing membranes (Fig. 9). Our environment-sensitive site-directed fluorescence approaches on NBD-labeled loop residues of the KvAP sensor (residues 110 to 117) clearly suggest that this crucial region of the sensor in DOPC/cholesterol membranes partitions at the membrane interface, which is a chemically heterogeneous region composed of lipid headgroups, water and portions of the acyl chain (Wiener and White, 1992). This is in agreement with the overall hydrophobic nature of this loop residues. Further, this membrane interfacial localization of the sensor loop is similar to our recent observations in zwitterionic and anionic membranes (Das et al., 2020; Das and Raghuraman, 2021). Interestingly, cholesterol modulates the structural dynamics of the sensor loop in membranes in a segmental fashion, *i.e.*, the residues 110 to 114 and 115 to 117 are influenced by cholesterol in different ways. For instance, environmental heterogeneity as indicated by lifetimes, rotational and hydration dynamics as revealed by anisotropy and REES measurements, respectively, suggests the dual nature of cholesterol's modulatory effect on the sensor loop residues. This could be due to cholesterol's known effects on the physical properties of membranes, which is indirect in nature, or direct cholesterol/protein interactions that modulate the conformational state of protein (Zakany et al., 2020).

It is known that cholesterol increases the water penetration in the interfacial region of DOPC membranes (Subczynski et al., 1994; Stubbs et al., 1995). In general, increase in the environmental polarity will substantially reduce both fluorescence intensity and lifetimes (Raghuraman et al., 2019; Brahma et al., 2022). We observed significant reduction in fluorescence intensity of NBD for all the NBD-labeled sensor residues in cholesterol-containing membranes (Fig. 2C), however, the lifetimes do not match with this trend (see Fig. 3B). In addition, the sensor residues are significantly shielded from water exposure, and, interestingly, the water accessibility of the loop residues remains almost similar for both PC/PG and DOPC/cholesterol membranes (see Fig. 4D). Yet, the dynamics of hydration is significantly altered by cholesterol (Fig. 5B). Considering the functional correlations of hydration and conformational dynamics in inactivating and conductive conformations of K^+ channels (Raghuraman et al., 2014; Kratochvil et al., 2016), our results showing the presence of restricted/bound water molecules in the immediate vicinity of the loop region might also be relevant for the sensor function. Moreover, it appears that the conformational heterogeneity of the KvAP sensor loop is affected by the presence of cholesterol in membranes.

Interestingly, our quantitative depth analysis by parallax method reveals that there is a modest decrease in membrane penetration depth for the sensor loop residues (~2 Å) in cholesterol-containing membranes, which is consistent with the modest movement of the S4 helix proposed by tilt-shift model for the lipid-dependent gating of KvAP (Li et al., 2014b). It should be noted that the sensor loop residues should have been partitioned deeper (*i.e*, increased membrane penetration depth) in membranes containing cholesterol (*i.e*, in the 'Down' state) had the S3b-S4 moves like a rigid body during 'Up'/activated to 'Down'/resting state of VSD. The fact that we observe decrease in membrane penetration depth in the presence of cholesterol clearly suggests that the paddle motif loop might adopt altered flexible organization, probably due to twisting around G114, with differential dynamics and may not be directly correlated with the direction of movement of S4 helix. Taken together, these results are supportive of the change in conformational state of the KvAP-VSD in cholesterol-containing membranes compared to PC/PG (Zheng et al., 2011; Jiang, 2019). Overall, our results bring out the importance of cholesterol in the organization and dynamics of S3b-S4 loop region of VSD, which might be relevant for the voltage- and lipid-dependent gating mechanisms and the effect of toxins on the modulation of sensor function in Kv channels.

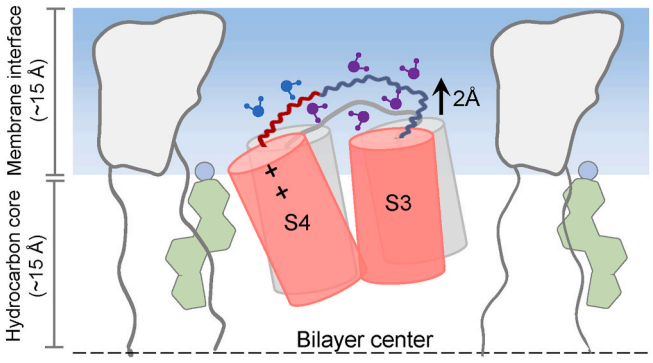

Fig. 9. Cholesterol-induced changes in the organization and dynamics of the voltage sensor loop. Schematic representation of the key differences in the structural dynamics of S3b-S4 loop residues of KvAP-VSD in PC/PG (grey), where the sensor adopts the 'Up' conformation and in cholesterol-containing DOPC membranes (red), where the 'Down' state conformation is stabilized. Only the upper leaflet of the bilayer is shown, and the dashed black line depicts the center of the bilayer. In both conformations, the sensor loop reside at the membrane interfacial region, which is a chemically heterogeneous region with a thermal thickness of ~15 Å is depicted as blue slab. Only a part of the S3b and S4 helices are shown as cylinders. The '+' symbols represent the gating charges of the S4 helix. The influence of cholesterol is not uniform throughout the loop as depicted by dual coloured loop and wiggly nature denotes the dynamic variability. The small v-shaped spheres represent membrane-associated water molecules and the changes in hydration dynamics of the loop are depicted by the presence of bulk/free (cyan) and restricted/bound (purple) water molecules. The cholesterol-induced modest change in the membrane penetration depth (~2 Å) of the sensor loop is shown with an upward black arrow. See Discussion for more details. (For interpretation of the references to colour in this figure legend, the reader is referred to the Web version of this article.)

CRediT authorship contribution statement

Anindita Das: Conceptualization, Methodology, Investigation, Formal analysis. **Arpan Bysack:** Methodology, Investigation, Formal analysis, Writing – review & editing. **H. Raghuraman:** Conceptualization, Supervision, Formal analysis, Writing – review & editing, Funding acquisition.

Declaration of competing interest

The authors declare that they have no known competing financial interests or personal relationships that could have appeared to influence the work reported in this paper.

Data availability

Data will be made available on request.

Acknowledgements

This work was supported by the Department of Atomic Energy, Government of India, and Department of Science and Technology, Government of India. H.R. thanks DST-SERB for the award of an Early Career Research Award (ECR/2016/001056), and is the recipient of the India Alliance DBT-Wellcome Intermediate Fellowship (IA/I/17/2/503321). A.D. and A.B. thank the Department of Biotechnology, Government of India, and Department of Atomic Energy, Government of India for the award of a Senior Research Fellowship, respectively.

References

Alabi, A.A., Bahamonde, M.I., Jung, H.J., Kim II., J., Swartz, K.J., 2007. Portability of paddle motif function and pharmacology in voltage sensors. Nature 450, 370–375.

Bellisent-Funel, M.C., Hassanali, A., Havenith, M., Henchman, R., Pohl, P., Sterpone, F., van der Spoel, D., Xu, Y., Garcia, A.E., 2016. Water determines the structure and dynamics of proteins. Chem. Rev. 116, 7673–7697.
Berezin, M.Y., Achilefu, S., 2010. Fluorescence lifetime measurements and biological imaging. Chem. Rev. 110, 2641–2684.
Bezanilla, F., 2008. How membrane proteins sense voltage. Nat. Rev. Mol. Cell Biol. 9, 323–332.
Bradberry, M.M., Bao, H., Loou, X., Chapman, E.R., 2019. Phosphotidylinositol 4,5-bisphosphate drives Ca2+-independent membrane penetration by the tandem C2 domain protein synaptotagmin-1 and Doc2β. J. Biol. Chem. 294, 10942–10953.
Brahma, R., Das, A., Raghuraman, H., 2022. Site-directed fluorescence approaches to monitor the structural dynamics of proteins using intrinsic Trp and labeled with extrinsic fluorophores. STAR Protoc 3, 101200.
Brahma, R., Raghuraman, H., 2021. Novel insights in linking solvent relaxation dynamics and protein conformations utilizing red edge excitation shift approach. Emerg. Top. Life Sci. 5, 89–101.
Brahma, R., Raghuraman, H., 2022. Measuring membrane penetration depths and conformational changes in membrane peptides and proteins. J. Membr. Biol. 255, 469–483.
Brahma, R., Raghuraman, H., 2024. Characterization of a novel MgtE homolog and its structural dynamics in membrane mimetics. Biophys. J. https://doi.org/10.1016/j.bpj.2023.11.3402.
Catacuzzeno, L., Franciolini, F., 2022. The 70-year search for the voltage-sensing mechanism of ion channels. J. Physiol. 600, 3227–3247.
Catterall, W.A., 2010. Ion channel voltage sensors: structure, function, and pathophysiology. Neuron 67, 915–928.
Chakrapani, S., Cuello, L.G., Cortes, D.M., Perozo, E., 2008. Structural dynamics of an isolated voltage-sensor domain in a lipid bilayer. Structure 16, 398–409.
Chatterjee, S., Brahma, R., Raghuraman, H., 2021. Gating-related structural dynamics of the MgtE magnesium channel in membrane-mimetics utilizing site-directed tryptophan fluorescence. J. Mol. Biol. 433, 166691.
Chattopadhyay, A., London, E., 1987. Parallax method for direct measurement of membrane penetration depth utilizing fluorescence quenching by spin-labeled phospholipids. Biochemistry 26, 39–45.
Chattopadhyay, A., Mukherjee, S., Raghuraman, H., 2002. Reverse micellar organization and dynamics: a wavelength-selective fluorescence approach. J. Phys. Chem. B 106, 13002–13009.
Corradi, V., Sejdiu, B.I., Mesa-Galloso, H., Abdizadeh, H., Noskov, S.Y., Marrink, S.J., Tieleman, D.P., 2019. Emerging diversity in lipid-protein interactions. Chem. Rev. 119, 5775–5848.
Crowley, K.S., Reinhart, G.D., Johnson, A.E., 1993. The signal sequence moves through a ribosomal tunnel into a noncytoplasmic aqueous environment at the ER membrane early in translocation. Cell 73, 1101–1115.
Cuello, L.G., Cortes, D.M., Perozo, E., 2004. Molecular architecture and local dynamics of the KvAP voltage-dependent K^+ channel in a lipid bilayer. Science 306, 491–495.
Das, A., Bysack, A., Raghuraman, H., 2021. Effectiveness of dual-detergent strategy using Triton X-100 in membrane protein purification. Biochem. Biophys. Res. Commun. 578, 122–128.
Das, A., Chatterjee, S., Raghuraman, H., 2020. Structural dynamics of the paddle motif loop in the activated conformation of KvAP voltage sensor. Biophys. J. 118, 873–884.
Das, A., Raghuraman, H., 2021. Conformational heterogeneity of the voltage sensor loop of KvAP in micelles and membranes: a fluorescence approach. Biochim. Biophys. Acta Biomembr. 1863, 183568.
Datta, R., Heaster, T.M., Sharick, J.T., Gillette, A.A., Skala, M.C., 2020. Fluorescence lifetime imaging microscopy: fundamentals and advances in instrumentation, analysis, and applications. J. Biomed. Opt. 25, 1–43.
de Meyer, F., Smit, B., 2009. Effect of cholesterol on the structure of a phospholipid bilayer. Proc. Natl. Acad. Sci. USA 106, 3654–3658.
Demchenko, A.P., 2008. Site-selective red-edge effects. Methods Enzymol. 450, 59–78.
Fery-Forgues, S., Fayet, J.-P., Lopez, A.J., 1993. Drastic changes in the fluorescence properties of NBD probes with the polarity of the medium: involvement of a TICT state? J. Photochem. Photobiol., A 70, 229–243.
Gunthrope, M.J., 2022. Timing is everything: structural insights into the disease-linked Kv3 channels controlling fast action-potential firing in the brain. Nat. Commun. 13, 4086.
Heberle, F.A., Feigenson, G.W., 2011. Phase separation in lipid membranes. Cold Spring Harbor Perspect. Biol. 3, a004630.
Ho, D., Lugo, M.R., Merrill, A.R., 2013. Harmonic analysis of the fluorescence response of bimane adducts of colicin E1 at helices 6, 7, and 10. J. Biol. Chem. 288, 5136–5148.
Hunte, C., 2005. Specific protein-lipid interactions in membrane proteins. Biochem. Soc. Trans. 33, 938–942.
Islas, L.D., 2016. Functional diversity of potassium channel voltage-sensing domains. Channels 10, 202–213.
James, N.G., Jameson, D.M., 2014. Steady-state fluorescence polarization/anisotropy for the study of protein interactions. In: Engelborghs, Y., Visser, A.J.W.G. (Eds.), *Fluorescence Spectroscopy And Microscopy: Methods And Protocols,* Methods in Molecular Biology. Spinger Science+Business Media, LLC, pp. 29–42.
Jiang, Q.-X., 2019. Cholesterol-dependent gating effects on ion channels. Adv. Exp. Med. Biol. 1115, 167–190.
Jiang, Q.-X., Gonen, T., 2012. The influence of lipids on voltage-gated ion channels. Curr. Opin. Struct. Biol. 22, 529–536.
Jiang, Y., Lee, A., Chen, J., Ruta, V., Cadene, M., Chait, B.T., MacKinnon, R., 2003. X-ray structure of a voltage-dependent K^+ channel. Nature 423, 33–41.
Johnson, A.E., 2005. Fluorescence approaches for determining protein conformations, interactions and mechanisms at membranes. Traffic 6, 1078–1092.
Kaiser, R.D., London, E., 1998. Location of diphenylhexatriene (DPH) and its derivatives within membranes: comparison of different fluorescence quenching analysis of membrane depth. Biochemistry 37, 8180–8190.
Kim, D.M., Nimigean, C.M., 2016. Voltage-gated potassium channels: a structural examination of selectivity and gating. Cold Spring Harbor Perspect. Biol. 8, a029231.
Kratochvil, H.T., Carr, J.K., Matulef, K., Annen, A.W., Li, H., Maj, M., Ostmeyer, J., Serrano, A.L., Raghuraman, H., Moran, S.D., Skinner, J.L., Perozo, E., Roux, B., Valiyaveetil, F.I., Zanni, M.T., 2016. Instantaneous ion configurations in the K^+ ion channel selectivity filter revealed by 2D IR spectroscopy. Science 353, 1040–1044.
Krishnamoorthy, G., 2018. Fluorescence lifetime distribution brings out mechanisms involving biomolecules while quantifying population heterogeneity. In: Geddes, C.D. (Ed.), Reviews in Fluorescence. Springer Nature Switzerland AG, pp. 75–98.
Kusumi, A., Tsunoyama, T.A., Tang, B., Hirosawa, K.M., Morone, N., Fujiwara, T.K., Suzuki, K.G.N., 2023. Cholesterol- and actin-centered view of the plasma membrane: updating the Singer-Nicolson fluid mosaic model to commemorate its 50th anniversary. Mol. Biol. Cell 34, pl1.
Kyrychenko, A., Vasquez-Montes, V., Ladokhin, A.S., 2022. Advantages of quantitative analysis of depth-dependent fluorescence quenching: case study of BAX. J. Membr. Biol. 255, 461–468.
Lau, C.H.Y., King, G.F., Mobli, M., 2016. Molecular basis of the interaction between gating modifier spider toxins and the voltage sensor of voltage-gated ion channels. Sci. Rep. 6, 34333.
Lee, A.G., 2003. Lipid-protein interactions in biological membranes: a structural perspective. Biochim. Biophys. Acta 1612, 1–40.
Lee, A.G., 2004. How lipids affect the activities of integral membrane proteins. Biochim. Biophys. Acta 1666, 62–87.
Lee, A.G., 2011. Biological membranes: the importance of molecular detail. Trends Biochem. Sci. 36, 493–500.
Lee, S.-Y., Lee, A., Chen, J., MacKinnon, R., 2005. Structure of the KvAP voltage-dependent K^+ channel and its dependence on the lipid membrane. Proc. Natl. Acad. Sci. USA 102, 15441–15446.
Lee, S.-Y., MacKinnon, R., 2004. A membrane-access mechanism of ion channel inhibition by voltage sensor toxins from spider venom. Nature 430, 232–235.
Levitan, I., Singh, D.K., Rosenhouse-Dantsker, A., 2014. Cholesterol binding to ion channels. Front. Physiol. 5, 65.
Li, Q., Wanderling, S., Paduch, M., Medovoy, D., Singharoy, A., McGreevy, R., Villalba-Galea, C.A., Hulse, R.E., Roux, B., Schulten, K., Kossiakoff, A., Perozo, E., 2014a. Structural mechanism of voltage-dependent gating in an isolated voltage-sensing domain. Nat. Struct. Mol. Biol. 21, 244–252.
Li, Q., Wanderling, S., Sompornpisut, P., Perozo, E., 2014b. Structural basis of lipid-driven conformational transitions in the KvAP voltage-sensing domain. Nat. Struct. Mol. Biol. 21, 160–166.
Li, T., Hassanali, A.A., Kao, Y.T., Zhong, D., Singer, S.J., 2007. Hydration dynamics and time scales of coupled water-protein fluctuations. J. Am. Chem. Soc. 129, 3376–3382.
Lin, S., Struve, W.S., 1991. Time-resolved fluorescence of nitrobenzoxadiazol-aminohexanoic acid: effect of intermolecular hydrogen bonding on non-radiative decay. Photochem. Photobiol. 54, 361–365.
Lingwood, D., Simons, K., 2010. Lipid rafts as a membrane-organizing principle. Science 327, 46–50.
London, E., Ladokhin, A.S., 2002. Measuring the depth of amino acid residues in membrane inserted peptides by fluorescence quenching. In: Benos, D., Simons, S. (Eds.), Current Topics in Membranes. Elsevier, San Diego, pp. 89–115.
Long, S.B., Tao, X., Campbell, E.B., MacKinnon, R., 2007. Atomic structure of a voltage-dependent K^+ channel in a lipid membrane-like environment. Nature 450, 376–382.
Marsh, D., 2010. Liquid-ordered phases induced by cholesterol: a compendium of binary phase diagrams. Biochim. Biophys. Acta 1798, 688–699.
Meza, U., Delgado-Ramirez, M., Romero-Mendez, C., Sanchez-Armass, S., Rodriguez-Menchaca, A.A., 2020. Functional marriage in plasma membrane: critical cholesterol level-optimal protein activity. Br. J. Pharmacol. 177, 2456–2465.
Mukherjee, S., Raghuraman, H., Chattopadhyay, A., 2004. Organization and dynamics of N-(7-nitrobenz-2-oxa-1,3-diazol-4-yl)-labeled lipids: a fluorescence approach. Chem. Phys. Lipids 127, 91–101.
Murata, Y., Iwasaki, H., Sasaki, M., Inaba, K., Okamura, Y., 2005. Phosphoinositide phosphatase activity coupled to an intrinsic voltage sensor. Nature 435, 1239–1243.
Ngoc, L.L.N., Pandey, R.B., Sompornpisut, P., 2021. Dynamics and environmental characteristics of spin labels in a KvAP voltage sensor by molecular dynamics simulations. J. Phys. Chem. B 125, 748–756.
Payandeh, J., Scheuer, T., Zheng, N., Catterall, W.A., 2011. The crystal structure of a voltage-gated sodium channel. Nature 475, 353–358.
Raghuraman, H., Chatterjee, S., Das, A., 2019. Site-directed fluorescence approaches for dynamic structural biology of membrane peptides and proteins. Front. Mol. Biosci. 6, 96.
Raghuraman, H., Chattopadhyay, A., 2007. Orientation and dynamics of melittin in membranes of varying composition utilizing NBD fluorescence. Biophys. J. 92, 1271–1283.
Raghuraman, H., Islam, S.M., Mukherjee, S., Roux, B., Perozo, E., 2014. Dynamics transitions at the outer vestibule of the KcsA potassium channel during gating. Proc. Natl. Acad. Sci. USA 111, 1831–1836.
Raghuraman, H., Shrivastava, S., Chattopadhyay, A., 2007. Monitoring the looping up of acyl chain labeled NBD lipids in membranes as a function of membrane phase state. Biochim. Biophys. Acta 1768, 1258–1267.
Ramu, Y., Xu, Y., Lu, Z., 2006. Enzymatic activation of voltage-gated potassium channels. Nature 442, 696–699.
Rao, M., Mayor, S., 2014. Active organization of membrane constituents in living cells. Curr. Opin. Cell Biol. 29, 126–132.

Roux, B., 2017. Ion channels and ion selectivity. Essays Biochem. 61, 201–209.
Ruta, V., Chen, J., MacKinnon, R., 2005. Calibrated measurement of gating-charge arginine displacement in the KvAP voltage-dependent K^+ channel. Cell 123, 463–475.
Ruta, V., Jiang, Y., Lee, A., Chen, J., MacKinnon, R., 2003. Functional analysis of an archaebacterial voltage-dependent K^+ channel. Nature 422, 180–185.
Schmidt, D., Jiang, Q.-X., MacKinnon, R., 2006. Phospholipids and the origin of cationic gating charges in voltage sensors. Nature 444, 775–779.
Shepard, L.A., Heuck, A.P., Hamman, B.D., Rossjohn, J., Parker, M.W., Ryan, K.R., Johnson, A.E., Tweten, R.K., 1998. Identification of a membrane-spanning domain of the thiol-activated pore-forming toxin *Clostridium perfringens* perfringolysin O: an α-helical to β-sheet transition identified by fluorescence spectroscopy. Biochemistry 37, 14563–14574.
Smith, D.A., McKenzie, G., Jones, A.C., Smith, T.A., 2017. Analysis of TCSPC data: a comparative evaluation of deterministic and probabilistic approaches. Methods Appl. Fluoresc. 5, 042001.
Stubbs, C.D., Ho, C., Slater, S.J., 1995. Fluorescence techniques for probing water penetration into lipid bilayers. J. Fluoresc. 5, 19–28.
Subczynski, W.K., Pasenkiewicz-Gierula, M., Widomska, J., Mainali, L., Raguz, M., 2017. High cholesterol/low cholesterol: effects in biological membranes review. Cell Biochem. Biophys. 75, 369–385.
Subczynski, W.K., Wisniewska, A., Yin, J.-J., Hyde, J.S., Kusumi, A., 1994. Hydrophobic barriers of lipid bilayer membranes formed by reduction of water penetration by alkyl chain unsaturation and cholesterol. Biochemistry 33, 7670–7681.
Swartz, K.J., 2007. Tarantula toxins interacting with voltage sensors in potassium channels. Toxicon 49, 213–230.
Swartz, K.J., 2008. Sensing voltage across lipid membranes. Nature 456, 891–897.
Sych, T., Levental, K.R., Sezgin, E., 2022. Lipid-protein interactions in plasma membrane organization and function. Annu. Rev. Biophys. 51, 135–156.
Taghon, G.J., Rowe, J.B., Kapolka, N.J., Isom, D.G., 2021. Predictable cholesterol binding sites in GPCRs lack consensus motifs. Structure 29, 499–506.
Takeshita, K., Sakata, S., Yamashita, E., Fujiwara, Y., Kawanabe, A., Kurokawa, T., Okochi, Y., Matsuda, M., Narita, H., Okamura, Y., Nakagawa, A., 2014. X-ray crystal structure of voltage-gated proton channel. Nat. Struct. Mol. Biol. 21, 352–357.
Tao, X., MacKinnon, R., 2019. Cryo-EM structure of the KvAP channel reveals a non-domain-swapped voltage sensor topology. Elife 8, e52164.
Tombola, F., Pathak, M.M., Isacoff, E.Y., 2006. How does voltage open an ion channel? Annu. Rev. Cell Dev. Biol. 22, 23–52.
Torbeev, V., 2020. Illuminating voltage sensor paddling in different membrane milieu. Biophys. J. 118, 781–782.
van Meer, G., Voelker, D.T., Feigenson, G.W., 2008. Membrane lipids: where they are and how they behave. Nat. Rev. Mol. Cell Biol. 9, 112–124.
Whicher, J.R., MacKinnon, R., 2016. Structure of the voltage-gated K^+ channel Eag1 reveals an alternative voltage sensing mechanism. Science 353, 664–669.
Wiener, M.C., White, S.H., 1992. Structure of fluid dioleoylphosphatidylcholine bilayer determined by joint refinement of x-ray and neutron diffraction data. III. Complete structure. Biophys. J. 61, 434–447.
Wulff, H., Castle, N.A., Pardo, L.A., 2009. Voltage-gated potassium channels as therapeutic targets. Nat. Rev. Drug Discov. 8, 982–1001.
Xu, Y., Ramu, Y., Lu, Z., 2008. Removal of phosphor-head groups of membrane lipids immobilizes voltage sensors of K^+ channels. Nature 451, 826–829.
Yeagle, P.L., 1985. Cholesterol and the cell membrane. Biochim. Biophys. Acta 822, 267–287.
Yeagle, P.L., 2022. Unraveling a mystery: why human cells require cholesterol. Sci. Adv. 8, eade5927.
Zakany, F., Kovacs, T., Panyi, G., Varga, Z., 2020. Direct and indirect cholesterol effects on membrane proteins with specific focus on potassium channels. Biochim. Biophys. Acta 1865, 158706.
Zhang, X., Ren, W., DeCaen, P., Yen, C., Tao, X., Tang, L., Wang, J., Hasegawa, K., Kumasaka, T., He, J., Wang, J., Clapham, D.E., Yan, N., 2012. Crystal structure of an orthologue of the NaChBac voltage-gated sodium channel. Nature 486, 130–134.
Zheng, H., Liu, W., Anderson, L.Y., Jiang, Q.-X., 2011. Lipid-dependent gating of a voltage-gated potassium channel. Nat. Commun. 2, 250.